RL-TR-96-99
Final Technical Report
July 1996

INVERTED OPTICAL MODULATORS FOR COMMUNICATIONS NETWORKS

University of Arizona

N. Peyghambarian

APPROVED FOR PUBLIC RELEASE; DISTRIBUTION UNLIMITED.

19960910 065

DTIC QUALITY INSPECTED 3

Rome Laboratory
Air Force Materiel Command
Rome, New York

DISCLAIMER NOTICE

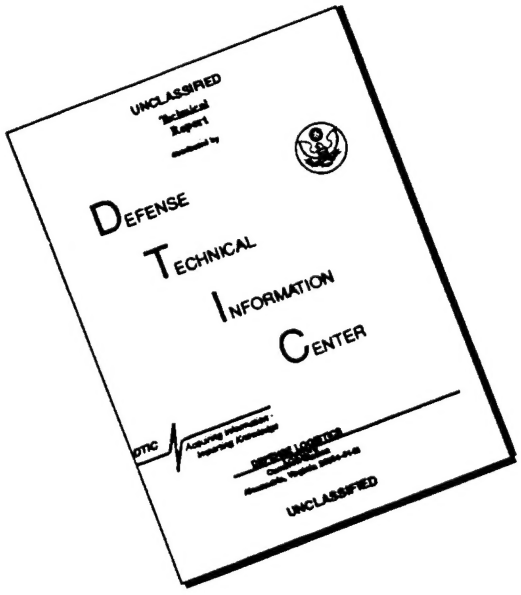

THIS DOCUMENT IS BEST QUALITY AVAILABLE. THE COPY FURNISHED TO DTIC CONTAINED A SIGNIFICANT NUMBER OF PAGES WHICH DO NOT REPRODUCE LEGIBLY.

This report has been reviewed by the Rome Laboratory Public Affairs Office (PA) and is releasable to the National Technical Information Service (NTIS). At NTIS, it will be releasable to the general public, including foreign nations.

RL-TR- 96-99 has been reviewed and is approved for publication.

APPROVED:

MARK F. KROL
Project Engineer

FOR THE COMMANDER:

GARY D. BARMORE, Major, USAF
Deputy Director of Surveillance & Photonics

If your address has changed or if you wish to be removed from the Rome Laboratory mailing list, or if the addressee is no longer employed by your organization, please notify Rome Laboratory/ (OCPA), Rome NY 13441. This will assist us in maintaining a current mailing list.

Do not return copies of this report unless contractual obligations or notices on a specific document require that it be returned.

REPORT DOCUMENTATION PAGE

Form Approved
OMB No. 0704-0188

Public reporting burden for this collection of information is estimated to average 1 hour per response, including the time for reviewing instructions, searching existing data sources, gathering and maintaining the data needed, and completing and reviewing the collection of information. Send comments regarding this burden estimate or any other aspect of this collection of information, including suggestions for reducing this burden, to Washington Headquarters Services, Directorate for Information Operations and Reports, 1215 Jefferson Davis Highway, Suite 1204, Arlington, VA 22202-4302, and to the Office of Management and Budget, Paperwork Reduction Project (0704-0188), Washington, DC 20503.

1. AGENCY USE ONLY (Leave Blank)	2. REPORT DATE	3. REPORT TYPE AND DATES COVERED
	July 1996	Final Jan 95 - Jan 96

4. TITLE AND SUBTITLE

INVERTED OPTICAL MODULATORS FOR COMMUNICATIONS NETWORKS

5. FUNDING NUMBERS

C - F30602-95-C-0006
PE - 62702F
PR - 4600
TA - P4
WU - PE

6. AUTHOR(S)

N. Peyghambarian

7. PERFORMING ORGANIZATION NAME(S) AND ADDRESS(ES)

University of Arizona
Arizona Board of Regents
2030 East Speedway Blvd
Tucson AZ 85721

8. PERFORMING ORGANIZATION REPORT NUMBER

N/A

9. SPONSORING/MONITORING AGENCY NAME(S) AND ADDRESS(ES)

Rome Laboratory/OCPA
25 Electronic Pkwy
Rome NY 13441-4515

10. SPONSORING/MONITORING AGENCY REPORT NUMBER

RL-TR-96-99

11. SUPPLEMENTARY NOTES

Rome Laboratory Project Engineer: Mark F. Krol/OCPA/(315)330-3634

12a. DISTRIBUTION/AVAILABILITY STATEMENT

Approved for public release; distribution unlimited.

12b. DISTRIBUTION CODE

13. ABSTRACT (Maximum 200 words)

The design and fabrication of a Kerr Lens Modelocked (KLM) chromium-doped forsterite laser is described. The KLM forsterite laser allows the study of ultrafast optical and electronic properties of materials in the near-IR with femtosecond time resolution. In particular, the laser produces sub-200 femtosecond pulses (tunable between 1240 and 1285 nm) with 2 kW of peak power at a 93 MHz repetition rate. The KLM forsterite laser was used in a degenerate pump-probe experiment to investigate the heavy-hole exciton dynamics of GaInAlAs/AlInAs multiple quantum wells. By tuning the laser to various wavelengths in the heavy-hole exciton region, both differential transmission and dephasing as a function of pump-probe delay were investigated. Ultrafast dynamics, such as the optical Stark effect, two-photon absorption, and absorption bleaching, were readily observed.

DTIC QUALITY INSPECTED 3

14. SUBJECT TERMS	15. NUMBER OF PAGES
Kerr lens modelocking, Chromium-doped forsterite laser, Exciton dynamics, Pump-probe spectroscopy, Multiple quantum wells	36
	16. PRICE CODE

17. SECURITY CLASSIFICATION OF REPORT	18. SECURITY CLASSIFICATION OF THIS PAGE	19. SECURITY CLASSIFICATION OF ABSTRACT	20. LIMITATION OF ABSTRACT
UNCLASSIFIED	UNCLASSIFIED	UNCLASSIFIED	UL

NSN 7540-01-280-5500

Standard Form 298 (Rev. 2-89)
Prescribed by ANSI Std. 239-18
298-102

TABLE OF CONTENTS

Abstract

A Kerr-lens mode-locked chromium doped forsterite laser was built allowing for the measurement of ultrafast dynamics of materials near the 1.25 μm wavelength region with subpicosecond time resolution. This laser is a self-mode-locking laser, producing sub-200 femtosecond pulses with 2 kW peak power at 93 MHz repetition rate tunable between 1240 and 1285 nm.

We measured exciton dynamics of GaInAlAs/AlInAs MQWs in the heavy-hole exciton region using the collinear degenerate pump and probe technique. By tuning our laser above and below the exciton resonance we were able to obtain the differential transmission and pump-probe dephasing as a function of pump-probe delay. Optical Stark effect, two-photon absorption and absorption bleaching are mechanisms readily observed.

Introduction

Optical fiber based communication networks are becoming more common in order to fulfill the growing demand for information capacity. For example, new services triggered by the large success of the internet are becoming available to the common public. These will necessitate an increased information capacity both in newly deployed optical fiber networks and already existing and upgradeable fiber networks. In order to more efficiently use the available bandwidth offered by optical fibers, techniques such as wavelength division multiplexing (WDM) and time-division multiplexing (TDM) are used. For the more recent generation of optical fiber networks operating at 1.55 μm, where the silica fiber has a propagation loss minimum and erbium-doped fiber amplifiers are available, dense WDM is probably the preferable technique. However, a substantial amount of the already deployed fiber networks are of previous generation. These operate at 1.3 μm where the group velocity dispersion reaches zero. The low group velocity dispersion allows for the propagation of very short pulses. Therefore, the upgrade of these networks is expected to profit from the use of TDM. Ultra-fast modulators are key components to TDM since direct modulation of laser diodes at the desired data rates introduces forbidding frequency chirp penalties.

In order to improve the performance of optical communications components, in particular, the time response of modulators, the fundamental processes limiting the speed of devices have to be investigated. Femtosecond pulsed lasers are therefore the tools of choice for the research and development of such devices.

Technical Report

Femtosecond Cr:Forsterite laser

Chromium doped forsterite ($Cr:Mg_2SiO_4$) was first demonstrated as a laser material by Petricevic et al. in 1988.[1] Its broad gain bandwidth made it a prospective candidate for ultrafast pulse generation, with hopes for a laser system similar to the Ti:sapphire.[2] However, the poor thermal conductivity and sharp decrease of fluorescence quantum efficiency with temperature attributed to phonon-assisted non-radiative decay has imposed some limitations on the Cr:forsterite laser system.[3] For this material demonstration of pulsed laser action[1] was rapidly followed by that of continuous wave operation,[4] wide tunability operation (1167 to 1345 nm when pumped by a Nd:YAG laser),[5] possibility of tunable multi-Watt cw output (at 77K),[3] and picosecond mode-locked operation.[6] Under mode-locked operation, and using intracavity prism pairs for group-velocity dispersion compensation sub-100-fs pulses were attained with active mode-locking[7] and regeneratively initiated mode-locking.[8] A different mechanism of mode-locking commonly termed Kerr-lens mode-locking (KLM) first observed in a Ti:Sapphire laser system[2] has generated great interest for solid-state laser mode-locking. It has been used to self-mode-lock several different lasers and has produced the shortest pulses obtained directly from a laser (8.5 fs in a Ti:sapphire).[9] Pulses as short as 25 fs have been produced in a Cr:forsterite laser system[10] using KLM together with optimized group-delay dispersion.

KLM is a form of passive mode-locking where no extra time modulating elements are used except for the lasing medium itself. In KLM, the high peak irradiance pulses are self-focused in the laser medium producing a mode profile with a different spot size than that of the cw mode. If the cavity is adjusted such that the overall loss for the pulsed mode is smaller than that for the cw mode, the laser can be made to self-pulsate. Self-sustained mode-locking (therefore the designation of self-mode-locking) with generation of ultra-short pulses is thus

possible provided that group-velocity dispersion (GVD) is compensated, so that soliton-type pulses propagate inside the cavity. Provided there is enough gain bandwidth, shorter pulses can be achieved when GVD compensation is optimized. To generate even shorter pulses higher order dispersion terms need to be compensated.[11] In KLM the discrimination between cw and pulsed operation by cavity adjustment is usually classified as hard-aperture mode-locking or soft-aperture mode-locking. In hard-aperture mode-locking an aperture is placed inside the cavity to create discriminating losses for the cw mode, whereas in soft-aperture mode-locking the pump mode and laser mode overlap provides for the discrimination. In general both types of KLM mode-locking may coexist. However, soft-aperture mode-locking is not always possible, as is the case for diode-pumped systems where the pump mode inside the lasing medium is much larger than the laser mode. In this sense, hard-aperture mode-locking seems to be a preferable technique given the possibility of modeling KLM lasers including this feature, thus providing a systematic way to build such ultrafast mode-locked lasers.

One of the most used tools for modeling laser cavities is the ABCD matrix formalism[12] used to describe beam propagation in paraxial optical systems. This formalism has been extended to include dispersive optical elements[13] and nonlinear effects such as self-focusing and self-phase modulation in a second-order theory (4×4 matrices).[14] However, with the advent of ever shorter pulses most of the modeling of KLM lasers has focused on the effects of higher order dispersion.[15] Another approach to KLM laser modeling has been developed by V. Magni et al.[16] towards hard-aperture KLM. It is based on the definition of a transfer matrix for the Kerr medium, consistent with the ABCD law for gaussian beams,[12] and the subsequent evaluation of a Kerr-lens sensitivity parameter dependent on cavity parameters.[16] This analysis has been extended to astigmatic resonators[17] and has lead to self-starting KLM of a Ti:sapphire laser.[17,18]

Laser Design

We have used an iterative procedure to design the cavity of our KLM Cr:forsterite as a hard-aperture KLM laser. The cavity is a Z-type cavity commonly used for KLM lasers as shown in Fig. 1. The steps in the design include the following:

1. assignment of distances between the elements in the cavity
2. numerical determination of the astigmatism compensation angle
3. stability check and mode spot size determination
4. numerical determination of the Kerr-lens sensitivity parameter
5. iteration from step 1 until design is adequate

We have also calculated the focal length of the pump focusing lens and its distance to the first curved mirror (M1) for mode-matching. Estimates of the prism separation in order to compensate for the group velocity dispersion in the cavity and of the third order dispersion were performed, as well as of losses due to Brewster angle dispersion of the prisms.

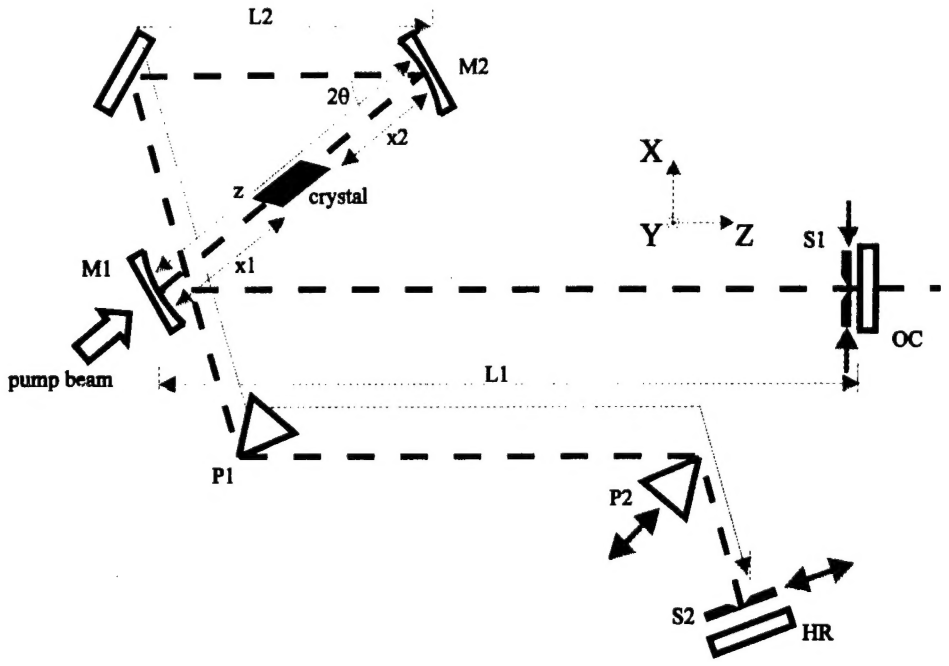

Figure 1. Cr:Forsterite laser with folded Z-cavity

The lasing material crystal is cut at Brewster angle in order to minimize reflection losses at the crystal-air interfaces thus avoiding the use of anti-reflection coatings. However, the Brewster cut geometry introduces astigmatism, as do the prisms used for group-velocity dispersion compensation. For the compensation of astigmatism the two curved focusing mirrors are set at an angle such that the output beam of the laser is non-astigmatic.

For the numerical determination of the astigmatism compensation angle an ABCD matrix program was used. The transfer matrices for the crystal, prisms and curved mirrors (set at an angle θ with respect to the normal) are different in the X (in plane or horizontal) and in the Y (out of plane or vertical) direction (see Fig. 1). Two cavities are defined, one for the X and another for the Y directions using the ABCD transfer matrices given in Refs. 12 and 19. This program uses a linear ABCD transfer matrix for the crystal, i.e., the Kerr effect is not taken into account at this point. The angle θ is left as a variable, and all the distances are assigned typical values. θ has to be such that the astigmatism introduced by the crystal and the prisms is compensated by the two curved mirrors (M1 and M2). The program uses an iterative algorithm to determine θ comparing the self-consistent gaussian beam solution for the X and Y cavities. It minimizes the difference in spot sizes (half-width 1/e of the field amplitude) in the X and Y directions for the arm of length L1 between mirror M1 and output coupler (OC). Consequently the beam coming out of the laser will also be circular. An initial good guess for the seed value input to the iterative algorithm is obtained from the equation[20]

$$2NL/R = 2\sin(\theta)\tan(\theta), \text{ with}$$

$$N = (n^2 - 1)/n^3,$$

where is the refractive index of the crystal at the wavelength of interest, L is the crystal length and R the radius of curvature of the focusing mirrors. (In the equation above a factor of 2 is introduced compared to the formula in Ref. 20 since we use two curved mirrors for the astigmatism compensation instead of one. Because of the different definition of crystal length a factor of

$$\sqrt{n^2 + 1}/n$$

is absent: we use the shortest distance between the Brewster cut crystal facets, and in Ref. 20 the element length is defined as the shortest distance normal to the facets). The θ determined numerically is then used in the subsequent steps of the cavity design process.

The geometrical stability[12] of the cavity in the X and Y directions is determined as a function of several cavity parameters using another program. As an example, Fig. 2 shows the stable region for our laser cavity as a function of distance x2, i.e., the crystal to mirror M2 distance (see Fig. 1). The stability region (here defined when the stability parameter assumes values between 0 and 1) is not the same in the X and Y directions. Only when the X and Y cavity stability regions overlap will the real cavity be stable in the geometrical sense. Fig. 2 shows that there are actually two stability regions, almost connected, since the Z-cavity used has nearly identical arm lengths (L1 and L2).

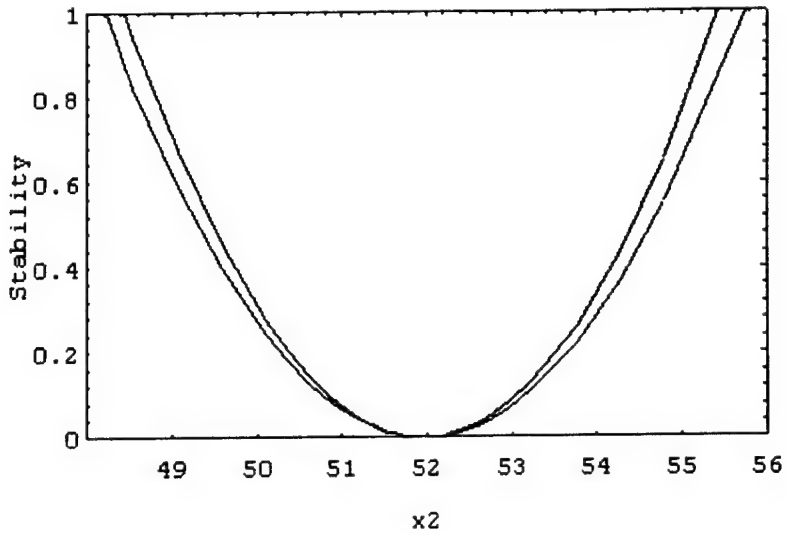

Figure 2. Stability parameters for the X and Y cavities as a function crystal to mirror M2 distance

Figures 3 to 5 show the beam radii evolution of the self-consistent gaussian beam solution for the X and Y cavities versus the linearized cavity length along the mode symmetry axis (the output coupler is at Z = 0, and the high reflector at the maximum Z). The vertical lines mark the position of the optical elements, the tilted interfaces and also the waist positions for the X and Y directions. Fig. 3 shows the beam radii evolution in the entire cavity; Fig. 4 shows the beam radii close to the crystal region where it is visible that the waists in the X and Y directions are not located at the same Z; Fig. 5 shows the beam radii near mirror M1 demonstrating that indeed the radii are the same for the output coupler arm, and therefore astigmatism is compensated.

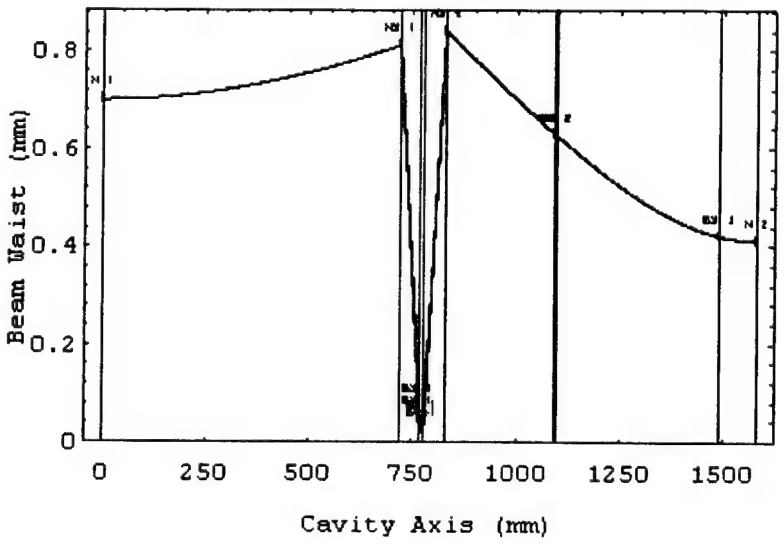

Figure 3. Beam spot size for the X and Y cavities

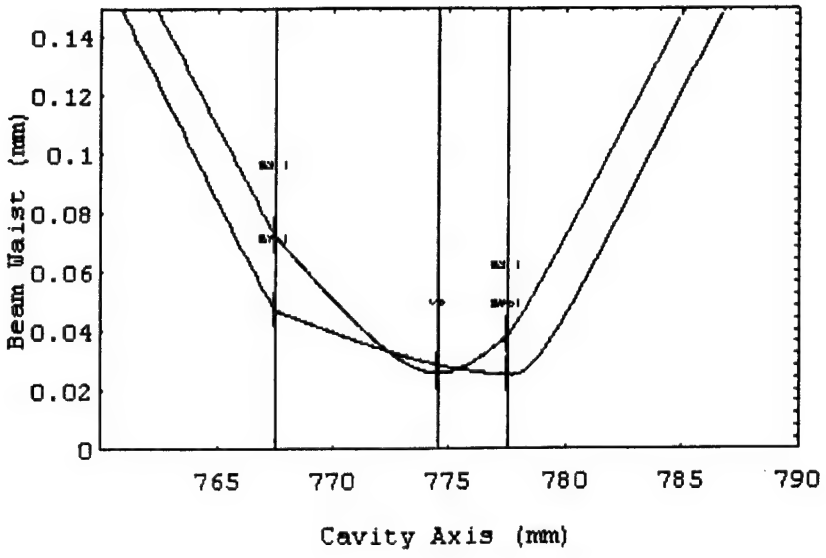

Figure 4. Spot sizes near the crystal region

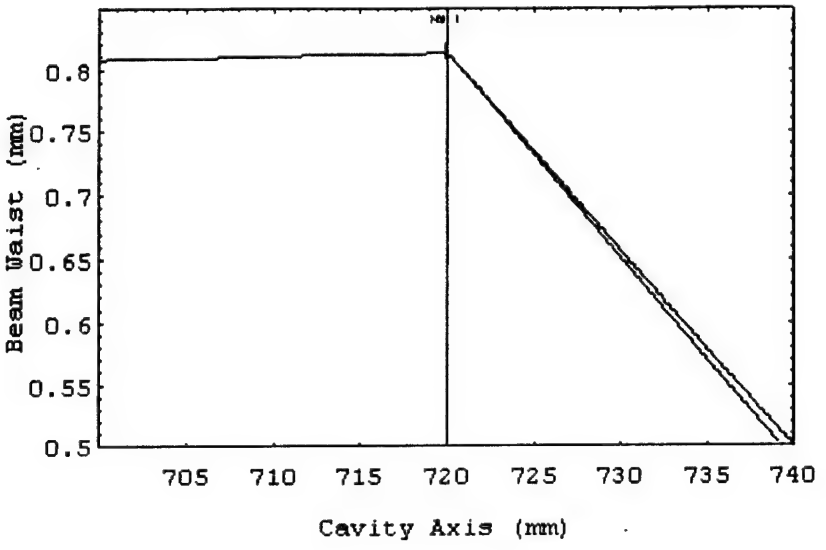

Figure 5. Spot sizes near mirror M1

In hard-aperture KLM lasers, the cavity losses due to an aperture are modulated by the instantaneous intracavity power. Assuming the TEM_{00} mode is not appreciably disturbed by the aperture a Kerr lens sensitivity parameter can be obtained proportional to the losses in first order. The loss of a gaussian beam through an aperture of width 2σ is given by

$$L = \frac{\int_a^\infty \exp[-2(r/w)^2]rdr}{\int_0^\infty \exp[-2(r/w)^2]rdr} = \exp[-2(\sigma/w)^2].$$

Therefore, to first order in power, the power dependent loss is given by

$$dL = 8(\sigma/w)^2 \exp[-2(\sigma/w)^2]p\delta .$$

The factor δ is the derivative of the beam spot size with respect to beam power, for vanishing power and at the plane where the aperture is located,

$$\delta = \left(\frac{1}{2w}\frac{dw}{dp}\right)\Bigg|_{p=0} .$$

The position of the aperture has to be such that δ is negative (decreasing losses with intracavity power) and large to self-mode-lock the laser. A large enough magnitude of δ can even make self-starting possible.[18] The largest magnitude of δ has been shown[17] to occur at the flat end mirrors (OC or HR), at an image of these or at their Fourier planes. We have chosen to place the hard-aperture slit (S1) near the output coupler.

The physical reasoning followed to obtain an expression for δ was to calculate the spot size variation at one of the flat end mirrors produced by a thin slice of Kerr lens medium, while neglecting the nonlinear effect of the remaining crystal. The total variation can be obtained by integrating over the length of the crystal. In Z-cavity type lasers, the Kerr medium is placed between two focusing mirrors, and the stability of the laser strongly depends on the distance between mirrors. Therefore, from a practical point of view, it is useful to express δ as a function of cavity geometry. V. Magni et al.[17] derived the following expression for δ_{OCx} (the δ parameter in the X direction calculated at the output coupler mirror)

$$\delta_{OCx} = \frac{-1}{n}\left(\frac{1-S_y^2}{1-S_x^2}\right)^{1/4} \int_0^L \left|\frac{B_{rtx}}{B_{rty}}\right|^{1/2} \frac{B_{2x}D_{2x}S_x + B_{1x}D_{1x}}{B_{rtx}^{\,2}} d\zeta ,$$

where ζ is the longitudinal coordinate in the Kerr medium; $B_{\pi x}$ and $B_{\pi y}$ are the (1,2) elements of the round trip matrices around the cavity from position ζ; B_{1x}, D_{1x} and B_{2x}, D_{2x} are the matrix elements for the propagation from position ζ to mirrors OC and HR respectively (see Fig. 1); and S_x, S_y are the stability factors for the X and Y directions, with $S_x = (A_{\pi x} + D_{\pi x}) / 2$ and similarly for S_y. Fig. 6 shows a detail of the contour plot for negative δ_{1x} as a function of the distance z between focusing mirrors, and the distance x1 from mirror M1 to the crystal (see Fig. 1) using the parameters of our laser. Fig. 7 shows the stability parameter for the same range of z. These two last figures show that the laser has to work close to the inner stability limit in order to self-mode-lock.

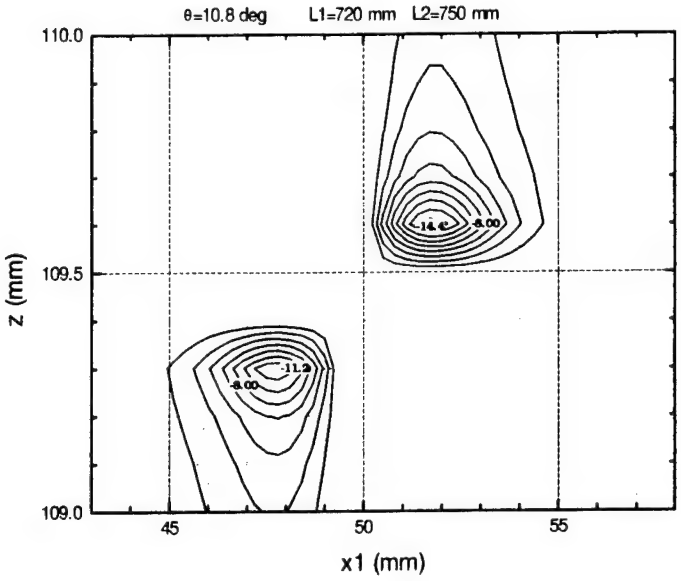

Figure 6. Kerr-lens sensitivity parameter δ - detail

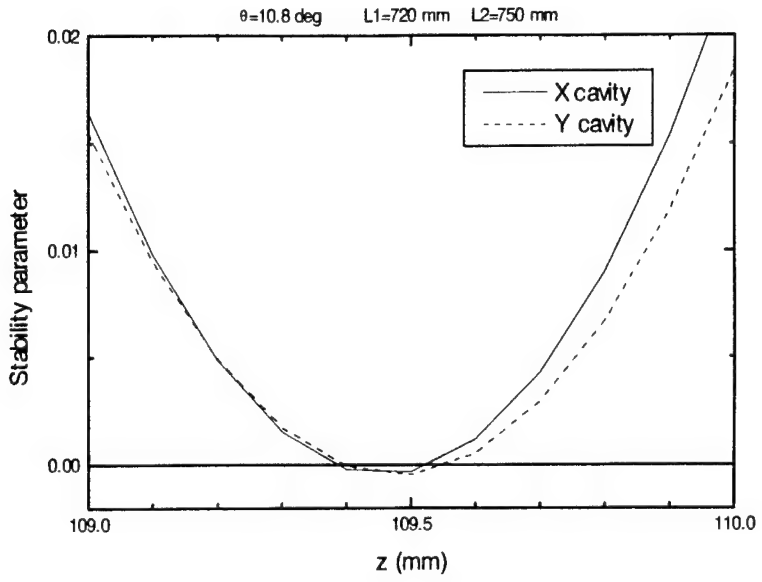

Figure 7. Stability parameter for the same stability region as Fig. 6

Figures 8 and 9 show the δ_{1x} contour plot over the full stability ranges for the ideal astigmatism compensation angle θ_{ideal} and for the angle $\theta_{non\text{-}ideal} = (\theta_{ideal} - 1 \text{ degree})$ respectively, demonstrating how sensitive the δ_{1x} map is to θ. Fig. 10 shows a detail of the stability parameter for $\theta_{non\text{-}ideal}$ defined above, showing that another forbidden region appears (stability parameter less than 0). These contour plots provide very useful guidelines for the adjustment of the laser cavity helping to obtain self-mode-locking.

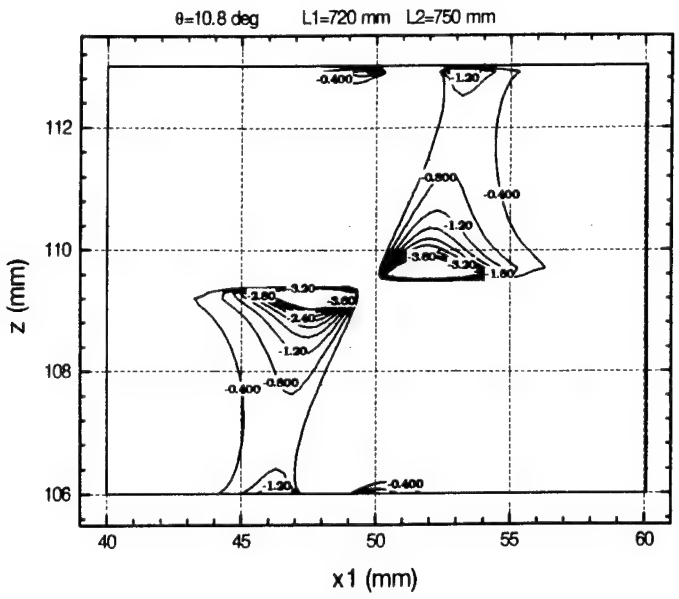

Figure 8. Kerr-lens sensitivity parameter δ - perfect astigmatic compensation

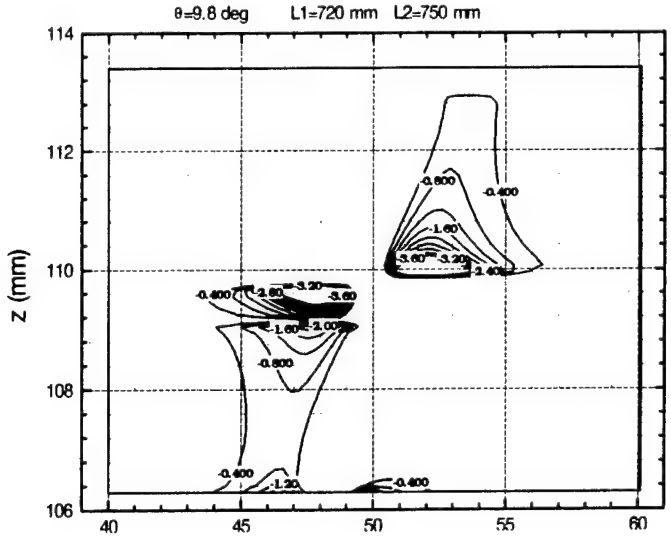

Figure 9. Kerr-lens sensitivity parameter δ - non-perfect astigmatic compensation

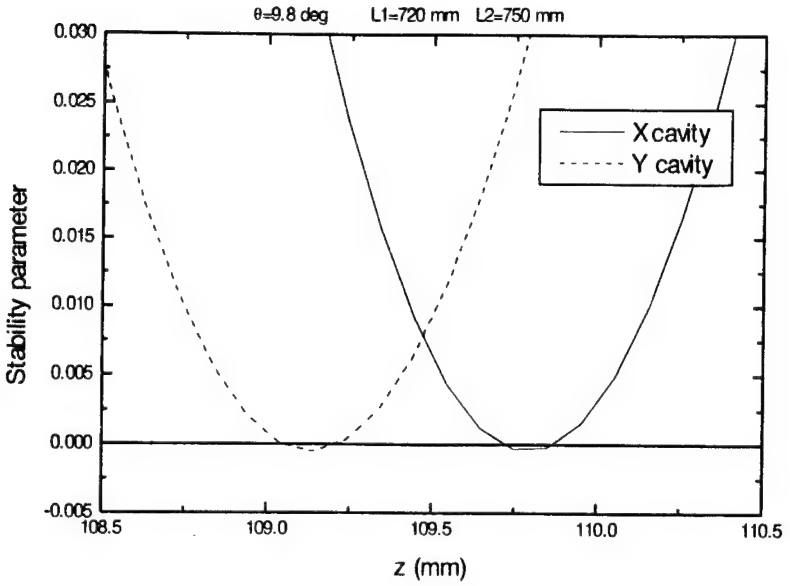

Figure 10. Stability parameter detail for non-perfect astigmatism compensation

Mode-matching of the pump beam and the laser beam inside the crystal is optimized for different focal length lenses available. With the help of a program the overlap is optimized and the best distance from the focusing lens to the back of mirror M1 determined. For a 15 cm lens the optimum is about 107 mm.

Solitary-type lasers are believed to produce the shortest pulses when the group velocity dispersion (GVD) the pulse experiences in a round trip is negative and has the smaller magnitude for which pulse formation is stable.[10] To obtain negative GVD grating pairs or prism pairs may be used. [11] The negative GVD introduced by the dispersing elements can be made to cancel the positive GVD due to the crystal. Prism pairs give both material dispersion and angular (also known as refractive) dispersion. The material dispersion adds positive GVD to that of the crystal. The angular GVD introduced can be calculated by analyzing the wavelength dependence of the optical path length through a prism pair such as that of Fig. 1. For Brewster prisms the derivation of an analytical formula is straightforward.[11] The second derivative of the optical path length with respect to wavelength is found to have two terms, with the negative term proportional

to the prism tip to tip distance. Therefore, for a long enough prism separation the angular dispersion provides negative GVD. Hence, by adjusting the prism separation the overall GVD can be compensated. In order to further shorten the pulses third order dispersion (TOD) needs to be taken into account. By choosing different combinations of prism materials and prism spacing TOD can be optimized for a certain wavelength while maintaining optimal GVD.[10,11]

Using the index of refraction dispersion for the Cr:Forsterite crystal obtained in Ref. 8, we have estimated the double pass material GVD and TOD introduced by the crystal to be 2500 fs^2 and 24000 fs^3 respectively. For the SF11 prism pair we have used the refractive index data provided in Ref. 22 and the Brewster prism assumption.[11] Assuming a total prism material insertion of 10 mm and 395 mm of prism separation, we calculate the material GVD and angular GVD introduced to be 900 fs^2 and -3700 fs^2 respectively. The estimated total GVD and total TOD are -300 fs^2 and 20000 fs^3 respectively.

We have also analyzed the influence of Brewster's angle dispersion of the prisms. Our SF11 prisms are cut at 60 deg. angles, and the Brewster's angle at 1265 nm is 60.255 deg. and varies less than 0.03 deg. through the 1200 to 1300 nm range. The round-trip transmission through the prism pair at 1265 nm is shown in Fig. 11.

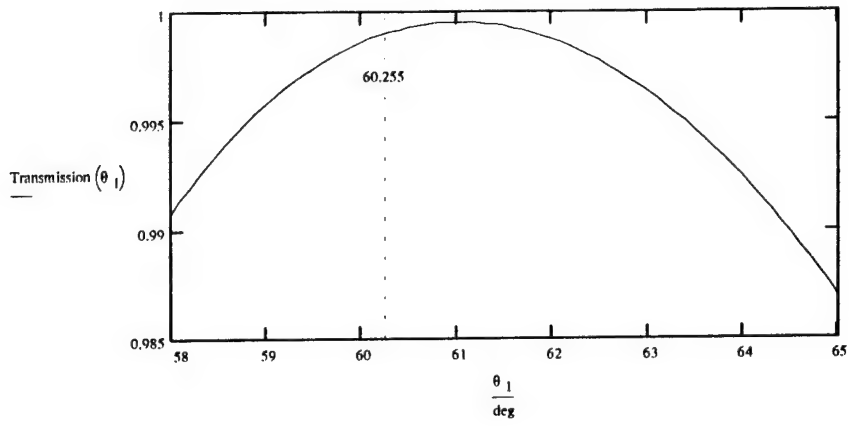

Figure 11. Round-trip transmission through the prism pair at 1265 nm

Laser parameters and characterization

The laser cavity is a Z-type cavity commonly used in KLM lasers (Fig. 12). The Cr:forsterite poor thermal conductivity and sharp decrease in fluorescence quantum efficiency with temperature, make imperative the use of some cooling system for the crystal. Our solution involves cooling the crystal by mounting it wrapped in indium foil on a brass slab. A pair of Peltier coolers placed between the crystal holding brass slab and a water cooled brass base keep the controlled temperature at around 3 ^{0}C.

A Spectra-Physics model 3800S cw Nd:YAG actively mode-locked laser is used as the pump source. This laser is capable of delivering over 10 W of 1064 nm 60 ps pulses at a repetition rate of 82.25 MHz. However, due to the thermal problems of the Cr:forsterite, the pump power is reduced to 7 W in order to self-mode-lock the laser. The long radiative decay time of the upper lasing level of ~3 μs at room-temperature[21] effectively averages the pump, and there is no observed 82.25 MHz modulation on the mode-locked Cr:forsterite laser output as measured with a rf-spectrum analyzer.

The components of the laser (Fig. 12) consist of a 10 mm long Brewster cut Cr:forsterite crystal,[21] two focusing mirrors with 100 mm radius of curvature, a flat 2% output coupler (OC), a flat high reflector (HR), and two 60 degrees SF11 prisms. Also, a flat high reflector folding mirror is used for compactness, as well as two slits for hard-aperture KLM (S1) and for tuning (S2). The refractive index of the Cr:forsterite crystal is ≈1.636,[21] and that of the prisms was obtained from Ref. 22.

The following procedure is followed when building the laser: The pump laser is kept at low powers in the early steps of alignment. The focusing lens, the pump focusing mirror (M1), the crystal at Brewster's angle and the second focusing mirror (M2) are inserted into the beam in this order and approximately at the distances obtained from the modeling. The OC and HR are inserted at the appropriate distances completing the first cavity (blue line — — --- in Fig. 12). The power from the Nd:YAG is increased so that the cavity can be aligned using the luminescence from the crystal. A mechanical chopper placed in the pump beam or in the arms of the cavity, together with a Ge or InGaAs photodetector after the HR or the OC may be used to assist in the alignment. Once lasing is achieved at high pump powers, the pump power is

reduced and the cavity alignment optimized to lower the pump power threshold. After minimizing the threshold pump power, the OC and tilt of mirrors M1 and M2 are not changed any further. A flat HR is used to fold the cavity for compactness and a second cavity is built and lasing optimized (green line – – – in Fig. 12). The prisms at near Brewster's angle and the HR are inserted using the remainder pump light for alignment, completing the final cavity (red line — — — in Fig. 12). The second and the final cavities can be made to lase simultaneously if prism P1 is adjusted to clip part of the second cavity lasing mode, providing another method of setting the final cavity . Once lasing is achieved the cavity is once again optimized. A variable slit (S1) is placed near the OC for hard-aperture KLM. Mode-beating is observed using a fast Ge detector connected to a 250 MHz sampling oscilloscope. By pushing on prism P2 (mounted on a translation stage), adjusting the slit (S1) and optimizing the cavity in agreement with the modeling, self-mode-locking is achieved. Mode-locking can also be observed in a slower oscilloscope, where a band will be observed instead of isolated pulses.

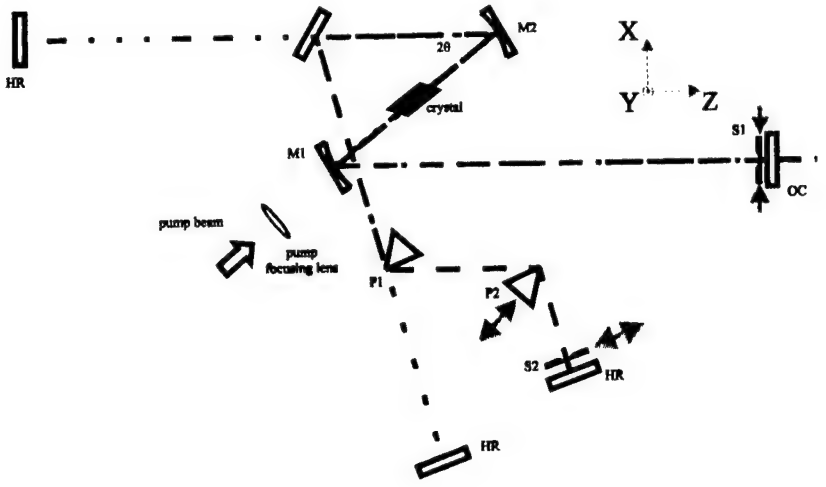

Figure 12. Cavities used to build the mode-locked Cr:Forsterite

The distances for our specific laser are (Fig. 1): M1 to crystal = x1 ≈ 48 mm; M2 to crystal = x2 ≈ 51 mm; M1 to OC = L1 ≈ 720 mm; M2 to HR = L2 ≈ 750 mm; P1 to P2 ≈ 395

mm. At 7 W pump power, mode-locked pulses are obtained as shown in Fig. 13 obtained with the 250 MHz sampling oscilloscope.

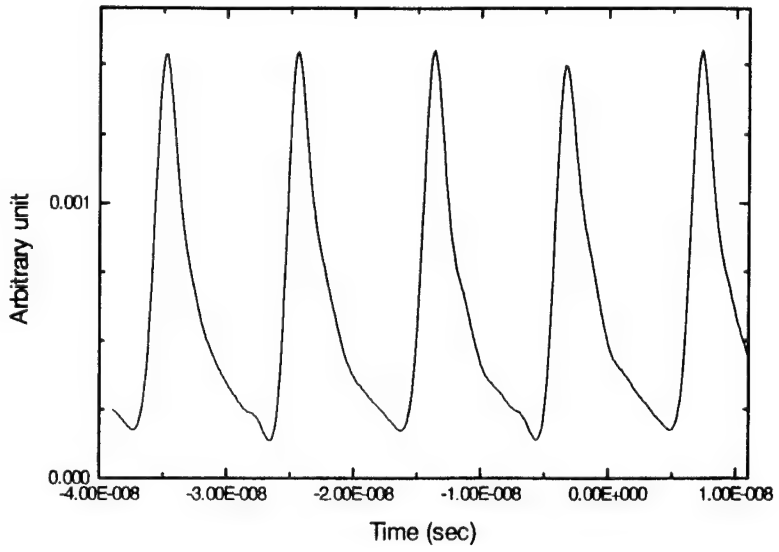

Figure 13. Cr:Forsterite pulses

As the femtosecond pulses cannot be resolved with a photodetector we use a home-made autocorrelator to determine the pulse width. The interferometric autocorrelation signal is given by

$$I(\tau) = \int_{-\infty}^{\infty} |\{E(t) + E(t-\tau)\}^2|^2 \, dt$$

and information on the pulse coherence is therefore available.[23] Fig. 14 shows a typical autocorrelation of the pulse. (The artifacts in the fringe pattern are due to the limited resolution in data transferring from the oscilloscope to the computer, and are not present in the original oscilloscope trace). The pulse width was determined by counting the number of fringes inside the FWHM upper envelope of the autocorrelation. The number of fringes together with the knowledge of the pulse central wavelength allows for the calculation of the pulse interferometric autocorrelation width. This is related to the actual pulse width by a factor of 1.897 for a $\text{sech}^2(t)$

pulse,[23] yielding a FWHM of 170 fs, and a time-bandwidth product of 1.09 times smaller than that for transform limited $sech^2(t)$ pulses, implying somewhat asymmetric pulses.

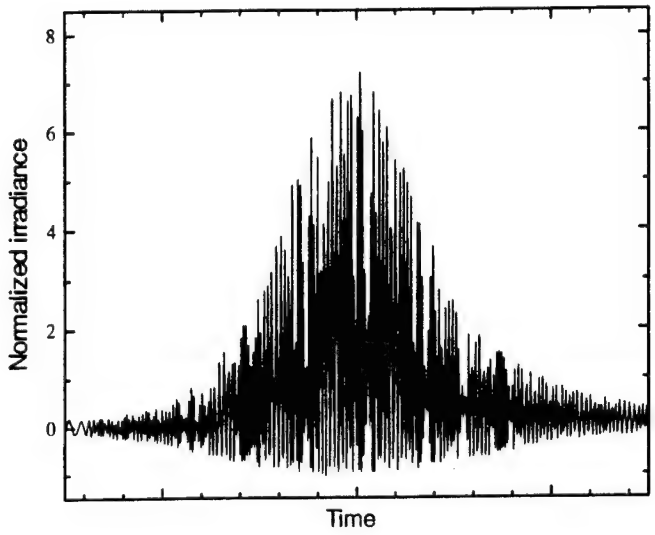

Figure 14. Interferometric autocorrelation

By introducing a slit (S2) near the HR we are able to tune the laser between 1240 and 1285 nm (see Fig. 15). Tuning is performed by sliding the slit along the X direction and adjusting the GVD compensation with prism P2 by introducing more or less glass in the beam path. The free-running laser (no tuning slit) tends to mode-lock near 1265 nm. The average output power is ≈30 mW at 7 W of pump power.

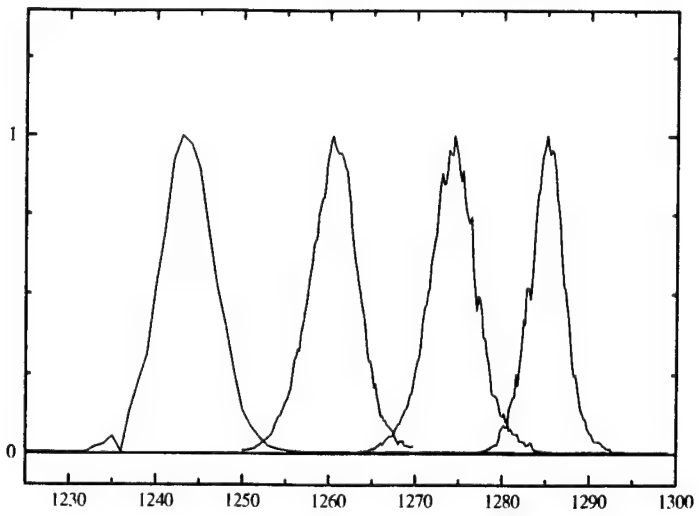

Figure 15. Tunability of mode-locked Cr:Forsterite laser

Time resolved exciton dynamics

Exciton dynamics of multiple quantum wells (MQW) were investigated with time-resolution given by our laser pulse width. The linear absorption spectrum of the GaInAlAs/ AlInAs MQW is presented in Figure 16.

We used a degenerate collinear cross-polarized pump-probe setup (Fig. 17). The output beam from the laser is divided into two by a polarizing beam-splitter, the power-ratio being controlled by the half-wave plate. The probe beam is recombined with the pump beam at the second beam-splitter. The variable time-delay is computer controlled using a stepper-motor in the delay-line which is synchronized with the data acquisition. A rotating variable neutral density filter which does not laterally displace the beam is placed in the pump beam arm to obtain variable pump power. A chopper is set to cut both the pump and probe beams but at different chopping frequencies. This allows for detection of signal due to the presence of both pump and probe (lock-in amplifier reference set at the sum of chopping frequencies), or by changing the reference frequency to the lock-in detect the signal just due to probe or pump. The

sample is placed inside a liquid nitrogen cryostat, at the focus of a 1:1 telescope. The horizontally polarized pump beam is eliminated after passing through the sample using a polarizer. Part of the beam is forwarded to the scanning spectrometer, and the remaining focused onto a InGaAs photodetector connected to the lock-in-amplifier. Zero-time delay is obtained with the sample removed. First, parallel fringes are obtained with the Cr:forsterite laser running cw. Then the motorized delay-line is set at a scanning speed that allows for fringe observation, the laser is mode-locked, and finally the delay-line is scanned until fringes are observed. The wavefront tilt is removed, the sample placed in the telescope focus, and the beam overlap at the sample optimized.

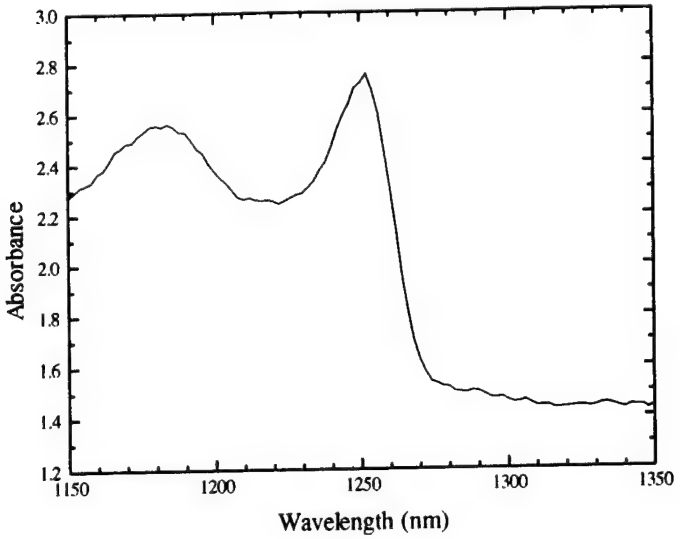

Figure 16. Linear absorption of GaInAlAs/AlInAs MQW

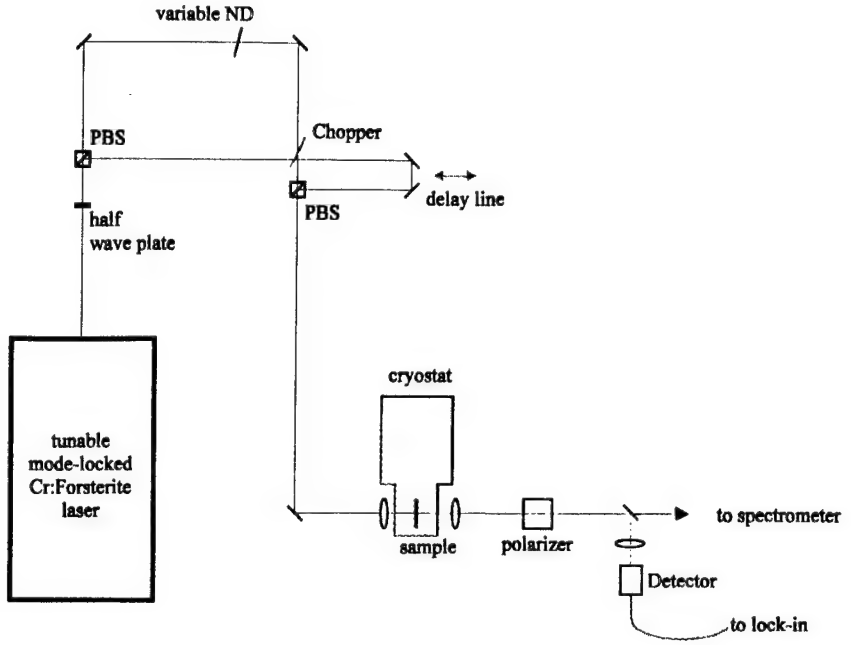

Figure 17. Pump-probe set-up

To obtain the differential transmission (DT) data, we tune the laser to the desired wavelength, adjust power in pump and probe beams, optimize overlap, and adjust the phase in the one channel lock-in amplifier. We have observed that the phase of the signal varies significantly with the time-delay between pump and pulse for wavelengths close to the exciton resonance, so that the phase adjustment is time-delay dependent. Therefore we took DT scans at two different phases at 90 degrees with respect to each other.

Figure 18 shows the probe differential transmission for pulses with different central wavelengths. From shorter to longer wavelengths, first we see only absorption bleaching at about one pulse bandwidth above the exciton; at the exciton resonance we see Stark effect, with a much larger differential signal; at just below the exciton two-photon absorption becomes visible since comparable to other effects; finally at about one pulse bandwidth below the exciton two-photon absorption dominates. Figure 19 shows the dephasing between pump and probe for pulses with central wavelengths corresponding to those in Figure 18.

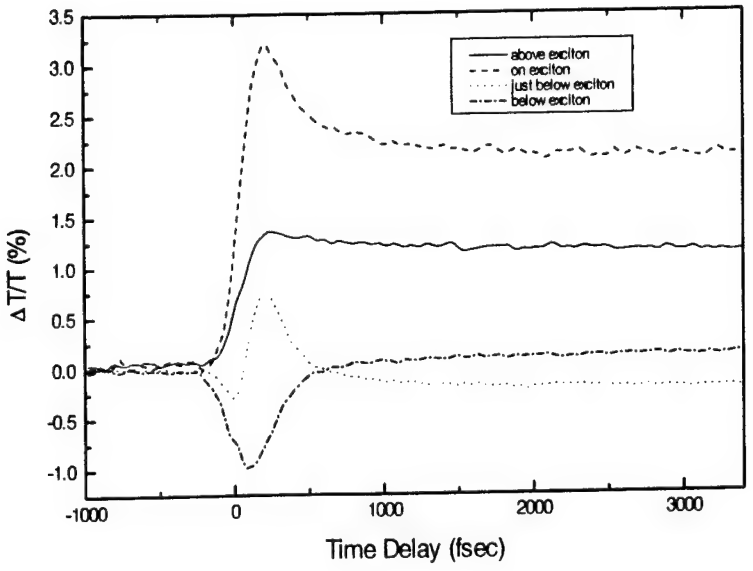

Figure 18. Pump differential transmission for several pulse wavelengths

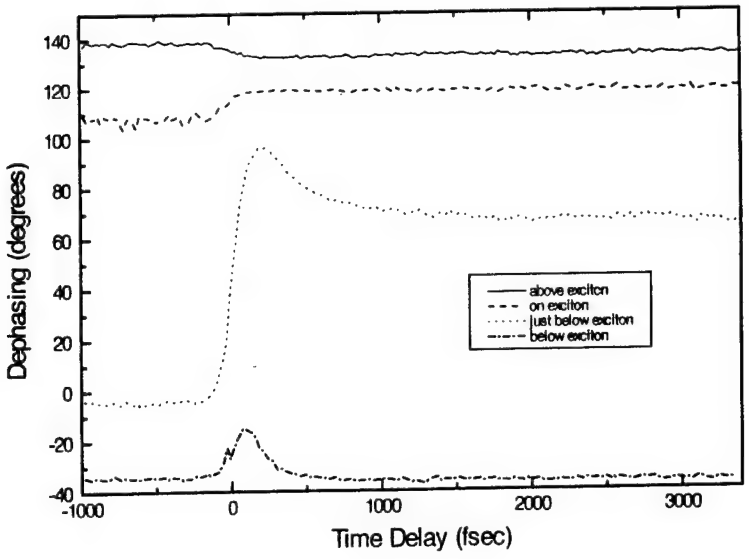

Figure 19. Pump-probe dephasing for several pulse wavelengths

Summary

In this project we built a hard-aperture self-mode-locked Cr:forsterite femtosecond laser following designing guidelines that should be extendible to other Kerr-lens mode-lockable laser systems. The laser output consists of sub 200 fs pulses at 93 MHz repetition rate tunable between 1240 and 1285 nm with 30 mW of average power. Higher power outputs should be possible with increased crystal cooling and better quality crystals. The exciton dynamics of GaInAlAs/AlInAs MQWs in the heavy-hole exciton region were investigated using collinear degenerate pump and probe with absorption bleaching, Stark effect and two-photon absorption apparent at different pulse wavelengths. Considerable pump-probe dephasing was observed for pulse wavelengths close to the exciton resonance.

References

1. V. Petricevic, S. K. Gayen, and R. R. Alfano, "Laser action in chromium-doped forsterite", Appl. Phys. Lett. **52** (13) 1040 (1988).
2. D. E. Spence, P. N. Kean, and W. Sibbett, "60-fsec pulse generation from a self-mode-locked Ti:sapphire laser", Opt. Lett. **16** (1) 42 (1991).
3. T. J. Carrig and C. R. Pollock, "Tunable, cw operation of a multiwatt forsterite laser", Opt. Lett. **16** (21) 1662 (1991).
4. V. Petricevic, S. K. Gayen, and R. R. Alfano, "Continuous-wave laser operation of chromium-doped forsterite", Opt. Lett. **14** (12) 612 (1989).
5. V. Petricevic, S. K. Gayen, and R. R. Alfano, "Near infrared tunable operation of chromium doped forsterite laser", Appl. Opt. **28** (9) 1609 (1989).
6. A. Seas, V. Petricevic, and R. R. Alfano, "Continuous-wave mode-locked operation of a chromium-doped forsterite laser", Opt. Lett. **16** (21) 1668 (1991).
7. A. Seas, V. Petricevic, and R. R. Alfano, "Generation of sub-100-fs pulses from a cw mode-locked chromium-doped forsterite laser", Opt. Lett. **17** (13) 937 (1992).
8. A. Sennaroglu, C. R. Pollock, and H. Nathel, "Generation of 48-fs pulses and measurement of crystal dispersion by using regeneratively initiated self-mode-locked chromium-doped forsterite laser", Opt. Lett. **18** (10) 826 (1993).
9. J. Zhou, G. Taft, C.-P. Huang, M. M. Murnane, H. C. Kapteyn, and I. P. Christov, "Pulse evolution in a broad-bandwith Ti:sapphire laser", Opt. Lett. **19** (15) 1149 (1994).
10. V. Yanovsky, Y. Pang, F. Wise, and B. I. Minkov, "Generation of 25-fs pulses from a self-mode-locked Cr:Forsterite laser with optimized group-delay dispersion", Opt. Lett. **18** (18) 1541 (1993).
11. R. L. Fork, C. H. Brito Cruz, P. C. Becker, and C. V. Shank, "Compression of optical pulses to six femtoseconds by using cubic phase compensation", Opt. Lett. **12** (7) 483 (1987); R. L. Fork, O. E. Martinez, and J. P. Gordon, "Negative dispersion using pairs of prims", Opt. Lett. **9** (5) 150 (1984); B. E. Lemoff and C. P. Barty, "Cubic-phase dispersion compensation in solid-state ultrashort-pulse lasers", Opt. Lett. **18** (1) 57 (1993).
12. See for example A. E. Siegman, "Lasers" (University Science Books, Mill valley, CA) 1986.
13. A. G. Kostenbauder, "Ray-pulse matrices: a rational treatment for dispersive optical systems", IEEE J. Quantum Electron. **26** (6) 1148 (1990).
14. O. E. Martinez and J. L. A. Chilla, " Self-mode-locking of Ti:sapphire lasers: a matrix formalism", Opt. Lett. **17** (17) 1210 (1992).
15. See for example H. A. Haus, J. D. Moores, and L. E. Nelson, "Effect of third-order dispersion on passive mode-locking", Opt. Lett. **18** (1) 51 (1993); I. P. Christov, M. M. Murnane, H. C. Kapteyn, J. Zhou, and C.-P. Huang, "Fourth-order dispersion-limited solitary pulses", Opt. Lett. **19** (18) 1465 (1994).
16. V. Magni, G. Cerullo, and S. De Silvestri, "ABCD matrix analysis of propagation of gaussian beams through Kerr media", Opt. Commun. **96** 348 (1993); — "Closed form gaussian beam analysis of resonators containing a Kerr medium for femtosecond lasers", Opt. Commun. **101** 365 (1993).

17. V. Magni, G. Cerullo, S. De Silvestri, and A. Monguzzi, "Astigmatism in gaussian-beam self-focusing and in resonators for Kerr-lens mode locking", J. Opt. Soc. Am. B **12** (3) 476 (1995).
18. G. Cerullo, S. De Silvestri, and V. Magni, " Self-starting Kerr-lens mode locking of a Ti:sapphire laser", Opt. lett. **19** (14) 1040 (1994).
19. J. -P. Taché, "Ray matrices for tilted interfaces in laser resonators", Appl. Opt. **26** (3) 427 (1987).
20. H. W. Kogelnik, E. P. Ippen, A. Dienes, and C. V. Shank, "Astigmatically compensated cavities for cw dye lasers", J. Quantum Electron. **8** (3) 373 (1972).
21. Mitsui Mining & Smelting Co., Ltd.; 2-1-1, Nihonbashi Muromachi, Chuo-Ku, Tokyo 103, Japan.
22. Schott Optical Glass Catalog.
23. J. -C. M. Diels, J. J. Fontaine, I. C. McMichael, and F. Simoni, "Control and measurement of ultrashort pulse shapes (in amplitude and phase) with femtosecond accuracy", App. Opt. **24** (9) 1270 (1985).

*U.S. GOVERNMENT PRINTING OFFICE: 1996-710-126-47010

MISSION

OF

ROME LABORATORY

Mission. The mission of Rome Laboratory is to advance the science and technologies of command, control, communications and intelligence and to transition them into systems to meet customer needs. To achieve this, Rome Lab:

a. Conducts vigorous research, development and test programs in all applicable technologies;

b. Transitions technology to current and future systems to improve operational capability, readiness, and supportability;

c. Provides a full range of technical support to Air Force Materiel Command product centers and other Air Force organizations;

d. Promotes transfer of technology to the private sector;

e. Maintains leading edge technological expertise in the areas of surveillance, communications, command and control, intelligence, reliability science, electro-magnetic technology, photonics, signal processing, and computational science.

The thrust areas of technical competence include: Surveillance, Communications, Command and Control, Intelligence, Signal Processing, Computer Science and Technology, Electromagnetic Technology, Photonics and Reliability Sciences.